Mariana Valéria de Araujo Sena ORCID iD: 0000-0003-4708-999X

Osteohistological characterization of notosuchian osteoderms: evidence for an overlying thick leathery layer of skin

Mariana Valéria de Araújo Sena[1,2*], Thiago da Silva Marinho[3,4], Felipe Chinaglia Montefeltro[5], Max Cardoso Langer[6], Thiago Schineider Fachini[6], William Roberto Nava[7], André Eduardo Piacentini Pinheiro[8], Esaú Victor de Araújo[9], Paul Aubier[1], Rafael César Lima Pedroso de Andrade[2], Juliana Manso Sayão[9], Gustavo Ribeiro de Oliveira[10], Jorge Cubo[1]

[1]Sorbonne Université, Muséum national d'Histoire naturelle, CNRS, Centre de recherche en paléontologie Paris (CR2P, UMR 7207), 4 Place Jussieu, Paris, BC 104, 75005, France mari.araujo.sena@gmail.com (corresponding author) (ORCID 0000-0003-4708-999X)

[2]Laboratório de Paleontologia da URCA - LPU, Centro de Ciências Biológicas e da Saúde, Universidade Regional do Cariri, Rua Carolino Sucupira – Pimenta, Crato, Ceará, 63105-010, Brazil

[3]Centro de Pesquisas Paleontológicas "Llewellyn Ivor Price", Complexo Cultural e Científico Peirópolis, Pró-Reitoria de Extensão Universitária, Universidade Federal do Triângulo Mineiro, Uberaba, Minas Gerais, 38039-758, Brazil

[4]Instituto de Ciências Exatas, Naturais e Educação (ICENE), Universidade Federal do Triângulo Mineiro (UFTM), Av. Randolfo Borges Jr. 1400, Univerdecidade, Uberaba, Minas Gerais, 38064-200, Brazil

[5]Departamento de Biologia e Zootecnia, Faculdade de Engenharia de Ilha Solteira, Universidade Estadual Paulista, Rua Monção, 226, Ilha Solteira, São Paulo, 15385-000, Brazil

[6]Laboratório de Paleontologia de Ribeirão Preto, Faculdade de Filosofia, Ciências e Letras de Ribeirão Preto, Universidade de São Paulo, Av. Bandeirantes, 3900, Ribeirão Preto, São Paulo, 14040-901, Brazil

This article has been accepted for publication and undergone full peer review but has not been through the copyediting, typesetting, pagination and proofreading process, which may lead to differences between this version and the Version of Record. Please cite this article as doi: 10.1002/jmor.21536.

[7]Museu de Paleontologia de Marília, Prefeitura Municipal de Marília, Av. Sampaio Vidal, 245, Marília, São Paulo, 17500-020 Brazil

[8]Faculdade de Formação de Professores (FFP), Universidade do Estado do Rio de Janeiro (UERJ), Campus São Gonçalo, Rua Dr. Francisco Portela, Bairro do Patronato, São Gonçalo, Rio de Janeiro, 24435-005, Brazil

[9]Museu Nacional do Rio de Janeiro, Universidade Federal do Rio de Janeiro, Quinta da Boa Vista s/nº, São Cristóvão, Rio de Janeiro, Rio de Janeiro, 20940-040, Brazil

[10]Laboratório de Paleontologia e Sistemática (LAPASI), Departamento de Biologia, Universidade Federal Rural de Pernambuco. Rua Dom Manoel de Medeiros, s/nº, Dois Irmãos, Recife, Pernambuco, 52171-900, Brazil

Abstract

Osteoderms are mineralized structures embedded in the dermis, known for non-avian archosaurs, squamates, xenarthrans and amphibians. Herein, we compared the osteoderm histology of Brazilian Notosuchia of Cretaceous age using three neosuchians for comparative purposes. Microanatomical analyses showed that most of them present a diploe structure similar to those of other pseudosuchians, lizards and turtles. This structure contains two cortices (the external cortex composed of an outer and an inner layers, and the basal cortex) and a core in-between them. Notosuchian osteoderms show high bone compactness (>0.85) with varying degrees of cancellous bone in the core. The neosuchian *Guarinisuchus* shows the lowest bone compactness with a well-developed cancellous layer. From an ontogenetic perspective, most tissues are formed through periosteal ossification, although the mineralized tissues observed in baurusuchid LPRP/USP 0634 suggest a late metaplastic development. Histology suggests that the ossification center of notosuchian osteoderm is located at the keel. Interestingly, we identified Sharpey's fibers running perpendicularly to the outer layer of the external cortex in *Armadillosuchus arrudai, Itasuchus jesuinoi* and Baurusuchidae (LPRP/USP

0642). This feature indicates a tight attachment within the dermis, and it is evidence for the presence of an overlying thick leathery layer of skin over these osteoderms. These data allow a better understanding of the osteohistological structure of crocodylomorph dermal bones, and highlight their structural diversity. We suggest that the vascular canals present in some sampled osteoderms connecting the inner layer of the external cortex and the core with the external surface may increase osteoderm surface and the capacity of heat transfer in terrestrial notosuchians.

Graphical Abstract

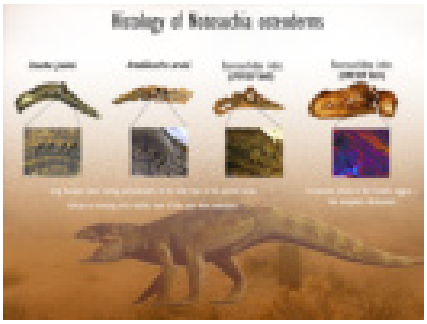

The perpendicular insertion of Sharpey's fibers in the external cortex suggests the presence of a thick leathery skin layer overlying notosuchian osteoderms.

Although intramembranous ossification is the main process involved in the development of crocodyliform osteoderms, we reported a case of metaplastic development.

Keywords: Ossification, osteoderm, osteohistology, Pseudosuchia.

Research Highlights

- The perpendicular insertion of Sharpey's fibers in the external cortex suggests the presence of a thick leathery skin layer overlying notosuchian osteoderms.
- Although intramembranous ossification is the main process involved in the development of crocodyliform osteoderms, we reported a case of metaplastic development.

1. INTRODUCTION

The reptile skin acts as an interface of the organism with the environment. It is composed of two layers, the epidermis and the dermis, separated by a fibrous membrane

(Nystrom & Bruckner-Tuderman, 2019). The outermost layer, the epidermis, is formed by three main strata: *stratum basale* or *germinativum* (inner), *stratum granulosum*, and *stratum corneum* (outer) (Rutland, Cigler & Kubale Dvojmoč, 2019). The underlying layer, the dermis, is bilaminar and organized into the s*tratum superficiale* and the *stratum compactum* (Williams et al. 2022). The dermis, where the osteoderms are located, includes blood vessels, cutaneous nerves, pigmentary cells, epidermic glandular tissues invaginating into the fibrous connective tissue (Rutland et al. 2019; Williams et al. 2022) and sometimes skeletal elements known as osteoderms.

Osteoderms are widespread integumentary features that occur in diverse extinct and extant amniotes, including turtles, non-avian archosaurs, lepidosaurs and cingulatan mammals (Burns, Vickaryous & Currie, 2013; Hill, 2005; Moss, 1972; Romer, 1956; Vickaryous & Sire, 2009; Witzmann, 2009). Osteoderms can bear superficial ornamentation in the dorsal surface, which may show different morphological patterns, such as tubercles in lizards, turtles, temnospondyls, and armadillos (Buffrénil, Dauphin, Rage & Sire, 2011; Scheyer et al. 2007; Sena et al. 2021; Vickaryous & Hall, 2006; Witzmann & Soler-Gijón, 2009), and pits and grooves in crocodylomorphs (Marinho, Ribeiro & Carvalho, 2006; Montefeltro, 2019). The osteohistology of osteoderms is heterogeneous (Vickaryous & Sire, 2009) comprising blood vessels, nerves, yellow marrow, a collagenous meshwork, and cancellous and cortical bone (Kirby et al. 2020; Moss, 1972; Vickaryous & Sire, 2009). Their microstructural organization reflects the mode of development, and it is useful to infer evolutionary patterns and test hypotheses of homology (Buffrénil et al., 2011). Osteoderms have a flexible resistant nature and Sharpey's fibers have a key role in anchoring them to the underlying musculature and connective tissue, thus contributing to the integrity of the skin (Chen, Yang & Meyers, 2014; Kirby et al. 2020; Scheyer et al. 2007). Some studies already proposed different functions for osteoderms besides protection, including mineral storage (Dacke et al.

2015) and thermoregulation (Farlow, Hyashi & Tattersall, 2010; Inacio Veenstra & Broeckhoven, 2022; Seidel, 1979).

Crocodylomorpha, an archosaur group with an evolutionary history from Late Triassic (Bronzati et al., 2015, Mannion et al. 2015) are characterized by the presence of osteoderms (Hill, 2005; Marinho et al. 2006; Montefeltro, 2019). Only few exceptions have been described, the most important being the absence of these structures in metriorhynchoids as an adaptation to a fully aquatic lifestyle (Ösi, Young, Galácz & Rabi, 2018). The spatial distribution of osteoderms in crocodylomorph bodies varies among groups. In Crocodylidae there are no osteoderm rows in the ventral surface, except by *Crocodylus johnstoni and C. cataphactus* (Burns, Vickaryous & Currie 2013; Brochu, 1999; Fuchs, 2006), whereas the extinct terrestrial *Simosuchus clarki* had a heavily armored body covered by osteoderms including dorsal and ventral surface of the body, as well as the limbs (Hill, 2010). In extant semi-aquatic Crocodylia osteoderms may help to stiffen the back to facilitate terrestrial locomotion (Salisbury & Frey, 2001; Molnar et al. 2014).

One of the most diverse groups of extinct crocodyliforms are the Notosuchia (sensu Ruiz et al. 2021), a clade of mostly terrestrial organisms limited to the Gondwanan landmasses during the Cretaceous. This group is characterized by a great diversity in osteoderms morphology, anatomy, and arrangements in the body ranging from the complete absence of osteoderm cover in *Pissarrachampsa sera* (Godoy et al. 2016; Montefeltro, 2019) to the extreme dorsal shield present in *Armadillosuchus arrudai* (Marinho & Carvalho, 2009). In this paper, we investigate the microstructure of notosuchian osteoderms based on the comparison of a sample coming from the Cretaceous and the Cenozoic of Brazil, and a few Neosuchia for comparative purposes. Moreover, we infer developmental aspects based on published data obtained for extant taxa.

Institutional abbreviations: CAV, Centro Acadêmico da Vitória Universidade Federal de Pernambuco, Vitória de Santo Antão, Brazil; CPPLIP, Centro de Pesquisas Paleontológicas "Llewellyn Ivor Price", Complexo Cultural e Científico de Peirópolis, Universidade Federal do Triângulo Mineiro, Peirópolis, Uberaba, Brazil; CR2P, Centre de Recherche en Paléontologie, Sorbonne Université, Paris, France; LAPASI, Laboratório de Paleontologia e Sistemática, Universidade Federal Rural de Pernambuco, Recife, Brazil; LAPEISA, Laboratório de Paleontologia e Evolução de Ilha Solteira, Universidade Estadual Paulista, Ilha Solteira, Brazil; LPRP/USP, Laboratório de Paleontologia, Universidade de São Paulo, Ribeirão Preto, Brazil; MCT, Museu de Ciências da Terra, Serviço Geológico do Brasil, Rio de Janeiro, Brazil; and MPM, Museu de Paleontologia de Marília, Marília, Brazil.

2. MATERIAL AND METHODS

Material

We performed thin-sections of 10 disarticulated osteoderms (seven notosuchians and three neosuchians; supplementary online material, Figure S1) as listed below:

- *Marialiasuchus amarali* Carvalho & Bertini, 1999. Partial osteoderm (MPM 087) from Late Cretaceous Bauru Group, Marilia–SP, Brazil.
- *Armadillosuchus arrudai* Marinho & Carvalho 2009. Partial osteoderm (LPRP/USP 0774) from Late Cretaceous Bauru Group, Jales–SP, Brazil.
- *Itasuchus jesuinoi* Price 1955. Complete osteoderm (CPPLIP 332) from Late Cretaceous Bauru Group, Uberaba–MG, Brazil.
- *Uberabasuchus terrificus* Carvalho, Ribeiro & Avilla 2004. Complete osteoderm (CPPLIP 501) from Late Cretaceous Bauru Group, Uberaba–MG, Brazil.
- *Aplestosuchus sordidus* Godoy, Montefeltro, Norell & Langer 2014. Complete osteoderm (LPRP/USP 0229-9) from the Uberaba-MG Bauru Group, General Salgado–SP, Brazil.

- Baurusuchidae indet. Two complete osteoderms (LPRP/USP 0634 and 0642) from Late Cretaceous Bauru Group, Brazil.
- Bernissartiidae indet. Fragmented osteoderm (LAPEISA 026) from Early Cretaceous, United Kingdom.
- *Caiman* sp. Complete osteoderm (LPRP/USP 0708, Castro et al. 2014) from the Pleistocene deposits at Ioiô cave Iraquara–BA, Brazil.
- *Guarinisuchus* cf. *G. munizi*, Barbosa, Kellner & Viana, 2008. Fragmented osteoderm (CAV 0013-V) from the Danian of Paraíba Basin, Brazil.

Sampling and methods for histological analysis

Samples were removed from each osteoderm to prepare the histological slides. Except for that of Bernissartiidae indet., the osteoderms were sectioned transversely (Clarac, Goussard, Teresi, Buffrénil, & Sansalone, 2017). Thin sections were prepared using standard fossil histology techniques (Chinsamy & Raath, 1992) at LAPAMI, CAV/UFPE and housed at the LAPASI, UFRPE. The specimens were embedded in clear epoxy resin Resapol T-208, catalyzed with Butanox M50 and cut with a diamond-tipped blade mounted on a saw. The mounting side of the sections was wet-ground using a metallographic polishing machine (Aropol-E, Arotec Ltda) with Arotec abrasive sandpapers of increasing grit size (80/P80, 320/P400, 1200/P1500) and grounded to a thickness 100-80 μm. Samples were observed using a petrographic polarizing microscope under normal and cross-polarized light with lambda compensator. Images were obtained using a Nikon Eclipse E600 POL microscope mounted to a Nikon Digital Sight DS-L 1, at CR2P. Our terminology follows Francillon-Vieillot et al. (1990) and Scheyer & Sander (2004).

Bone compactness analysis

We transformed photographs of the thin sections into binary images using Adobe Photoshop® CS6. This method marks the bone tissue in black and vascular spaces

(medullary cavity, vascular canals and resorption cavities) in white. The binary images (supplementary online material, Figure S2) were quantitatively analyzed in R using the Bone Profile R package, (Girondot & Laurin, 2003; Gônet, Laurin & Girondot, 2022) to calculate the compactness parameters.We quantified the bone compactness (ratio between the surface occupied by bone tissues and the total bone surface (Laurin et al., 2004), as well as the relative width of the transition zone between the medulla and the cortex (S), the distance of this transition zone from the center of the sections (P), and the minimum (Min) and maximum (Max) values of bone compactness (Girondot & Laurin, 2003) (supplementary online material, Table S1).

3. RESULTS

Osteohistological descriptions

Most osteoderms possess superficial ornamentations on their external surface, which consists of shallow rounded pits or deep elongated grooves or sulci, whereas their basal surfaces are smooth. The general microstructural corresponds to the diploe structure, i. e., a central cancellous core framed by compact cortices, with different degrees of remodeling and the presence of cancellous bone. All osteoderms show high bone compactness (Buffrénil, Sire & Rage, 2010).

Armadillosuchus arrudai (LPRP/USP 0774)

Although fragmentary, this osteoderm is well preserved, with its dorsal surface strongly ornamented (Figure 1A) by pits and four vascular canals connecting the inner and outer layers of the external cortex to the surfaceFigure. The thin section shows a high level of bone compactness (0.873). The external cortex exhibits a ridged pattern with depressions. This cortex is formed by an outer thin layer of an almost avascular parallel-fibered bone tissue with flattened rows of osteocyte lacunae. One resorption line separates the outer and the inner layers of the external cortex (Figure 1B). This cortex incorporates long Sharpey's fibers, i.e., mineralized in growing fibrillary processes from

adjacent soft bone tissues (Francillon-Vieillot et al., 1990, p. 504), which are perpendicularly projected to the external surface (Figure 1C). The core is composed of woven bone with abundant osteocyte lacunae which are densely arranged and vascularized by reticular vascular canals (Figure 1F). It contains portions of remodeled bone with irregular erosion cavities and secondary osteons surrounded by lamellar bone (Figure 1D). The basal cortex reveals periodic growth, with parallel-fibered bone tissue interrupted by growth marksFigureFigure 1G. The osteocyte lacunae have a round shape in both woven and parallel-fibered matrix. However, a flattened aspect is observed in the lamellar matrix (Figure 1F and 1G). Vascularization mainly consists of simple or anastomosed vascular canals and scarce primary osteons.

Insert Figure 1 here

Itasuchus jesuinoi (CPPLIP 332)

This osteoderm presents ornamentation composed of pits and grooves (Figure 2A) and a bone compactness of 0.967. The external surface shows a smooth pattern of valleys and ridges. The outer layer of the external cortex consists of lamellar-zonal bone tissue interrupted by closely spaced growth marksFigure. A resorption line is observed as the boundary between the outer and the inner layers of the external cortex. The vascular network is composed of a few simple or anastomosed primary vascular canals. Long Sharpey's fiber bundles are observed perpendicular to the external surface (Figure 2B). Osteocyte lacunae are elongated and orientated parallel to the fiber's orientation. The core presents a woven matrix with some portions of fibrolamellar tissue (Figure 2D), which is well-vascularized by primary osteons. The osteocyte lacunae are abundant and rounded in shape. Remodeling is identified by scattered secondary osteons (Figure 2E). The basal cortex is composed of parallel-fibered bone tissue interrupted by growth marks and vascularized by some primary osteons and reticular vascular canals (Figure 2C). Osteocyte lacunae show a flattened or irregular aspect oriented in parallel rows.

Insert Figure 2 here

Mariliasuchus amarali (MPM 087)

The superficial ornamentation of the osteoderm is formed by deep grooves, rare pits and vascular canals opening up from the inner core to the external surface (Figure 3A). The thin section shows a bone compactness of 0.857. The osteoderm exhibits a diploe structure and the cortices have similar thicknesses. The core is composed of heavily remodeled bone with numerous resorption cavities and secondary osteons surrounded by lamellar bone tissue (Figure 3D and 3E). The basal and external cortices are thin and formed by parallel-fibered and woven bone tissues vascularized by anastomosed and longitudinal vascular canals (Figure 3B and 3C). The osteocyte lacunae have either irregular or round shapes, randomly distributed. Figure.

Insert Figure 3 here

Uberabasuchus terrificus (CPPLIP 501)

The external cortex bears some depressions, which form the superficial ornamentation composed by pits and grooves above the parallel-fibered bone tissue layer (Figure 4A). The osteoderm presents a high bone compactness degree of 0.989. The inner core is composed of woven bone (Figure 4B) tissue, vascularized by anastomosed and longitudinal vascular canals and primary osteonsFigure; other portions show osteoclastic activity in the form of erosion cavitiesFigure. In these parts, osteocyte lacunae are more abundant and they are randomly distributed. Scarce secondary osteons are present in the core toward the basal cortex (Figure 4E), which is thicker than the external cortex and it is composed of parallel-fibered bone tissue and interrupted by growth marks and poorly vascularized (lamellar-zonal bone tissue) (Figure 4D). Osteocyte lacunae are less numerous than in the inner core, they also have a flat appearance oriented in parallel rows; short Sharpey's fibers cross perpendicularly the growth marks (Figure 4C).

Insert Figure 4 here

Aplestosuchus sordidus (LPRP/USP 0229-9)

This is a keeled osteoderm, with no superficial ornamentation and bone compactness of 0.920 (Figure 5A). The basal and external cortices are formed by parallel-fibered bone tissue with a reticular and longitudinal vascular pattern (Figure 5B and 5E). The basal cortex is thicker than the external one. The core presents some resorption cavities surrounded by remodeled lamellar bone tissue (Figure 5C). The growth marks are deposited in the cortices and core with some of them obliterated by remodelingFigure. The osteocyte lacunae present either irregular or round shape and they follow the fibers orientation forming subparallel rows. The cortical bone incorporated Sharpey's fibers with oblique orientation, probably to keep the adhesion among osteodermsFigure.

Insert Figure 5 here

Baurusuchidae indet. (LPRP/USP 0634 and 0642)

LPRP/USP 0634 is an osteoderm with a smooth ridge in the dorsal region and no superficial ornamentation and a bone compactness of 0.948 (Figure 6A). The basal and external cortices are well-vascularized showing a reticular and radial vascular pattern (Figure 6B). Some anastomosed vascular canals open towards the outer bone surface. The primary bone is mainly composed of woven and parallel-fibered bone. The inner region presents Haversian bone formed by different generations of secondary osteons (Figure 6C and 6D) surrounded by lamellar bone tissue. Abundant Sharpey's fibers are embedded in the primary cortex but show no preferential orientation. Inner cortical portions are composed of parallel-fibered bone tissue which preserves few LAGs (Figure 6E). These growth marks look obliterated by the remodeling process in the inner core (Figure 6D). The Osteocyte lacunae present round or irregular shapes that are abundant in the woven bone tissue. These cell lacunae exhibit a highly disorganized arrangement even in the parallel-fibered bone tissue.

Insert Figure 6 here

LPRP/USP 0642 exhibits a superficial ornamentation composed of shallow pits. A foramen canal connects the osteoderm core to the external surface (Figure 7A). The thin section reveals a high bone compactness of 0.912. The external cortex is formed by parallel-fibered bone tissue. A circular cavity is seen in the central core of the keel (Figure 7B) surrounded by secondary lamellar bone tissue Figure. A few growth marks are visible in some surfaces of the external parts, but these are more abundant in the basal cortex. Primary, parallel-fibered bone tissue vascularized by reticular vascular canals composes some portions of osteoderm core (Figure 7D)Figure. This region also presents scattered secondary osteons and erosion cavities surrounded by lamellar bone tissue. Some erosion cavities are anastomosed and others are concentrated towards the superficial keel. The basal cortex is formed by parallel-fibered bone tissue interrupted by growth marks (Figure 7E). Abundant bundles of Sharpey's fibers have diverse orientations, i.e., parallel, oblique or perpendicular towards the surface, in the compact cortex surface (Figure 7C). In the cortices, osteocyte lacunae possess an elongated or irregular aspect, and their arrangement follows the orientation of intrinsic fibers in which they are embedded.

Insert Figure 7 here

Bernissartiidae indet. (LPRP/USP 026)

Adiploe structure with a bone compactness of 0.956 is observed (Figure 8A). It is formed by a compact cortex, which is less vascularized than the inner region. The central core is mainly formed by small primary osteons and longitudinal vascular canals (Figure 8B). The cortices consist of woven bone tissue with abundant rounded or irregular osteocyte lacunae, randomly distributed (Figure 8C). The cortices are poorly vascularized by primary osteons, longitudinal or anastomosed vascular canals. The dark color of the

thin section is probably due to impregnation of iron oxides during the fossil diagenetic processes.

Insert Figure 8 here

Caiman sp. (LPRP/USP 0708)

This is an ornamented and keeled osteoderm and its compactness reaches 0.963 (Figure 9A). A foramen is observed near the basis of the keel, crossing the entire external cortex (Figure 9B). The basal cortex and most of the core present iron oxides impregnations from the fossil diagenesis and its microstructural pattern cannot be completely assessed. In the visible portions, the compact external cortex is formed by lamellar-zonal bone tissue with a parallel-fibered bone matrix interrupted by several growth marks (Figure 9C and 9E). The cortical bone is poorly vascularized with the presence of scattered primary osteons (Figure C). The core shows resorption cavities and secondary bone tissues sectioned in different orientations (Figure 9D). Osteocyte lacunae show elongated or irregular aspect, following orientation of the fibers in the primary bone tissue.

Insert Figure 9 here

Guarinisuchus cf. *G. munizi* (CAV 0013-V)

Both cortices are narrow and formed by avascular parallel-fibered bone tissue (Figure 10B). The cancellous bone is the largest layer; it is constituted by thin and long trabeculae (Figure 10A), intertrabecular spaces and erosion cavities (Figure 10D). The walls of the trabeculae bone constitute secondary lamellar bone lining vascular spaces and the primary interstitial bone areas within the trabeculae (Figure 10E). Osteocyte lacunae show different shapes, they are flattened in the secondary lamellar bone tissue of the inner core, irregular in the primary parallel-fibered bone tissue and rounded in the primary interstitial bone tissue (Figure 10C–E).

Insert Figure 10 here

4. DISCUSSION

General microstructural pattern

We sampled osteoderms with distinct external morphologies from different body positions. *Itasuchus* (dorsal), *Uberabasuchus* (dorsal) and *Armadillosuchus* (dorsal accessory) show a reduced cancellous layer. *Guarinisuchus* presents thin cortices and a well-developed secondary cancellous bone with long and slender trabeculae. The structure of baurusuchid LPRP/USP 0634 is similar to Baurusuchidae (MPMA 62.0002.02; Marchetti et al. 2022) characterized by the presence of cancellous bone containing small erosion cavities and highly vascularized cortices. The cancellous bone in Bernissartiidae osteoderm (indeterminate position) has a primary origin similar to the Aetosaurinae paramedian plate, MLP 61-VIII-2-34 (Cerda & Desojo, 2011). The inner core is the most histologically diverse layer besides the remodeled bone; it could present portions of parallel-fibered or fibrolamellar bone tissues (Figure 2D). Scheyer et al. (2014) indicated that the remodeling degree is directly related to the external ornamentation of the osteoderms. We did not observe this pattern in our sample since the highest degrees of remodeling was found in the scarcely ornamented *Guarinisuchus* osteoderm, while well-ornamented osteoderms (*Caiman* sp., *Armadillosuchus arrudai* and *Uberabasuchus terrificus*) show lower degree of resorption and secondary bone deposition.

Most of the osteoderms investigated in this study possess a diploe structure containing two cortices, the external and the basal cortices, and a core between them. This structure is similar to that observed in xenarthran osteoderms (Vickaryous & Hall, 2006), early tetrapods (Witzmann & Soler-Gijón, 2009), the aetosaurs *Calyptosuchus wellesi* and *Stagonolepis olenkae* (Scheyer et al., 2014); raiusuchians (Scheyer & Desojo, 2011) and turtle shell bones (e.g., Sena, Bantim, Saraiva, Sayão & Oliveira 2021; Skutschas, Boitsova, Cherepanov & Danilov, 2017). This pattern differs from that

observed in the Aetosaurinae specimens described by (Cerda & Desojo, 2011) and in the doswelliid *Tarjadia ruthae* dermal plates (Ponce et al., 2017), which lack the cancellous bone layer, and from the pareiasaurians (Scheyer & Sander 2009), which exhibit a spongy osteoderm. In the osteoderms studied here, the cortices display a homogenous aspect formed by parallel-fibered with some cyclical growth marks. The bone compactness of these Notosuchia specimens is higher than 85% included in the range of bone compactness of pseudosuchian osteoderms from 0.987 to 0.660 (e.g., Cerda, Desojo & Scheyer, 2018; Ponce, Cerda, Desojo & Nesbitt, 2017). *Armadillosuchus arrudai* presents the lowest bone compactness among notosuchians analyzed. Scheyer & Sander (2009) reported that the association of bone compactness and lifestyle is controversial for amniote osteoderms. In crocodyliforms, the bone compactness seems to have no influence on their lifestyle. It is probably related to the extension of osteoderm covering of the body. For instance, the dermal plates in *Simosuchus clarki* (Hill, 2010) and *Guarinisuchus* are extremely porous and lightly constructed. This high degree of porosity might be biomechanically relevant because it decreases the weight of the armor, ensuring its mobility as proposed by Chen et al. (2014) for *Alligator*.

The osteoderms of *Uberabasuchus terrificus*, *Itasuchus jesuinoi*, *Armadillosuchus arrudai*, *Mariliasuchus amarali* and Baurusuchidae indet. (LPRP/USP 0642) have basal cortices similar to those of aetosaurs, other pseudosuchian, and turtle shell plates (Scheyer et al. 2007; Sena, Bantim, Saraiva, Sayão & Oliveira, 2020; Sena et al. 2021). They are composed of parallel-fibered bone tissue poorly vascularized interrupted by growth marks.

However, *Aplestosuchus sordidus* and Baurusuchidae indet. (LPRP/USP 0634) show highly vascularized basal cortices, similar to those of phytosaur osteoderms (Scheyer, Desojo & Cerda,. 2014, Figure 5D). The vascular pattern in the osteoderms of bernissartiid resembles that of the Aetosaurinae, which was interpreted as a true

fibrolamellar complex (Cerda & Desojo, 2011, Figure 3E). However, we could not assess whether this dermal plate of bernissartiid presents fibrolamellar bone tissue due to the impregnation of the bone matrix by iron oxides from the fossildiagenesis.

The structure of Sharpey's fibers varies between the external and basal cortices. In the external cortex these fibers are long and thick while in the basal cortex they are shorter, thinner and more abundant intercepting growth marks. This pattern is also recognized in other extinct and extant archosaurs and turtles (e.g., Buffrénil et al. 2015; Hill, 2010; Sena, Andrade, Sayão & Oliveira, 2018; Woodward, Horner & Farlow, 2014). This pattern reflects the connection between the basal cortex and *stractum compactum* of the dermis (Burn et al., 2013) and suggests a tight anchorage of the osteoderm within the dermis (Scheyer et al. 2007). Sharpey's fibers are inserted perpendicularly to the external surface of the bone in the external cortices of *Armadillosuchus arrudai, Itasuchus jesuinoi* and Baurusuchidae indet. (LPRP/USP 0642). It suggests that during postembryonic growth, pre-existing collagen bundles of the dermis are incorporated perpendicularly into the element. The presence of Sharpey's fibers perpendicular to the outer layer of the external cortex is recorded also in recent trionychid turtle shell bones, in the marine turtle *Dermochelys coriacea* (Scheyer et al. 2007) and in the extinct aetosaur *Stagonolepis olenkae* (ZPAL Ab III/2379) (Scheyer, Danilov, Sukhanov & Syromyatnikova, 2014). We suggest that this feature is associated with the presence of a leathery dermis layer covering the osteoderms, similar to that covering the shell plates of recent soft-shelled turtles and the marine leatherback turtle. Because of that we suggest that *Armadillosuchus arrudai, Itasuchus jesuinoi* and baurusuchid indet. (LPRP/USP 0642) also had their dermal bones firmly anchored within the dermis covered by a leathery layer. This feature should increase the flexibility of their dermal armor as proposed by Chen, Yang & Meyers (2015) for *Dermochelys coriacea*.

Osteoderm skeletogenesis

At least three different ossification mechanisms were already proposed for the formation of reptile osteoderms and scute plates: metaplastic ossification (Scheyer & Sander, 2004), intramembranous ossification (von Baczko et al. 2019) and fibrocartilaginous ossification (Scheyer, 2007). Here, we propose that most notosuchian osteoderms sampled show the intramembranous ossification similar to what has been described in *Riojasuchus tenuisceps* (von Baczko et al., 2019), where a periosteal layer replaces a primary non-cartilaginous connective tissue. Portions of structural fibers found in the osteoderms of the Baurusuchid indet. (LPRP/USP 0634) can be interpreted as metaplastic tissue as proposed by Scheyer & Sander (2004) for ankylosaur osteoderms and Scheyer & Sánchez-Villagra (2007) for the turtle shells. The metaplastic development, which is the direct transition from the dermis into mineralized tissue (*sensu* Beresford, 1981), is rare for squamate (Vickaryous, Meldrum & Russell, 2015; Williams et al. 2022) and archosaur (Scheyer & Sander, 2004; Vickaryous & Hall, 2008) osteoderms. Also, it is worth noting that, unlike lizards, crocodyliform osteoderms do not regenerate (Vickaryous et al., 2015; Williams et al., 2022). In contrast, metaplasia is the main ossification type of shell plates of some turtle taxa (Sena et al., 2020; Scheyer & Sánchez-Villagra, 2007). Finally, metaplasia in Baurusuchidae indet. (LPRP/USP 0634; Figure 6F) seems to have occurred after the initial step of intramembranous ossification, as postulated by Vickaryous & Hall (2006) for *Dasypus*. Our findings corroborate Dubansky & Dubansky (2018) results suggesting that intramembranous ossification is the main process involved in the development of crocodyliform osteoderms.

According to von Baczko et al. (2019) the intramembranous ossification appears to be involved with the origin of osteoderms in Pseudosuchia being observed in early stages of osteoderms development, and also in basal group (Cerda et al. 2018), whereas the metaplastic ossification is more unusual. The osteoderms studied here also present a plesiomorphic set of growth pattern typical of turtles and crocodiles, represented by the

lamellar zonal bone composing the basal cortex (Klein, 2010), i.e., parallel-fibered and/or lamellar bone matrix showing several cyclical growth marks (see Francillon-Vieillot et al., 1990).

In addition, similar to turtle shells, the Baurusuchidae indet. (LPRP/USP 0642) and the *Caiman* sp. osteoderms present an isolated and enlarged circular space situated in the keel (Figures 7B and 9A). Such vascular canals are interpreted as the ossification centers of the osteoderms and are seen in shell plates of the extinct *Araripemys barretoi* (Sena et al. 2021), *Heckerochelys romani* (Scheyer et al. 2014), the testudinatan *Condorchelys antiqua* (Cerda, Sterli, Scheyer, 2016) and the extant *Podocnemis expansa* (Vieira et al. 2016) turtles. Osteoderms have a late ontogeny; they develop after the postcranial skeleton has formed within the well-differentiated dermis (Vickaryous & Hall, 2006). Similar to the formation of alligator osteoderm begins with calcium mineralization at the center (keel region) and proceeds radially, one year after hatching; calcium is gradually deposited on the collagen fibers from the surrounding dermis layer (Vickaryous & Hall, 2008).

5. CONCLUSION

The osteohistological data presented here suggest that notosuchian osteoderms are conservative regarding their microstructure. They show features like lamellar-zonal growth and mainly intramembranous ossification. Nonetheless, mineralized structural fibers were identified in osteoderms of baurusuchid (LPRP/USP 0634) indicating the contribution of metaplastic mineralization of collagenous fibers during skeletogenesis. Also, the presence of long and dense Sharpey's fibers perpendicular to the external cortex of *Armadillosuchus arrudai, Itasuchus jesuinoi* and Baurusuchid indet. (LPRP/USP 0642) osteoderms suggest their tight anchorage to an overlying leathery dermis layer increasing the dermal armor flexibility.

Acknowledgements

We thank D. Germain, curator of the Vertebrate Hard Tissue Collection of the Centre de Recherche en Paleontologie – Paris (MNHN, CNRS and Sorbonne Université), Dr A. Houssaye, CNRS professor, and Dr A. Herrel, head of the Function and Evolution team of the Unite Mixte de Recherche UMR 7179 (MNHN) for permitted acquisition of the pictures in their laboratories. We also thank the reviewers Dr T. Scheyer and an anonymous reviewer for their comments and suggestions that helped improve the quality of the manuscript. We also thank Fundação Cearense de Apoio ao Desenvolvimento Científico e Tecnológico (FUNCAp) and Conselho Nacional de Desenvolvimento Científico e Tecnológico (CNPq) for financial support grants. This research was supported by Sorbonne Université (Projet Emergences 2019 N° 243374 to J. Cubo).

Author contributions

Mariana Sena: Formal analysis (lead); funding acquisition; investigation (lead); methodology (lead); writing—original draft (lead); writing—review and editing (lead). **Thiago S Marinho**: Investigation; resources; writing-original draft; writing-review and editing. **Felipe C Montefeltro**: Investigation; resources; writing-original draft; writing-review and editing. **Max C Langer**: Investigation; resources; writing-original draft; writing-review and editing. **Thiago Schineider Fachini**: Investigation; resources; writing-original draft; writing-review and editing. **William R Nava:** Investigation; resources; writing-original draft; writing-review and editing. **Andre E. Piacentini Pinheiro**: Investigation; resources; writing-original draft; writing-review and editing. **Esau Victor de Araujo**: **Paul Aubier**: Investigation; resources; writing-original draft; writing-review and editing. **Rafael Cesar Pedroso Andrade**: Investigation; resources; writing-original draft; writing-review and editing. **Juliana Manso Sayao**: Investigation; resources; writing-original draft; writing-review and editing. **Gustavo Ribeiro de Oliveira**: Investigation; resources; writing-original draft; writing-review and editing.

Jorge Cubo: Conceptualization (lead); funding acquisition (lead); methodology (equal); project administration (lead); supervision (equal); writing—review and editing (lead).

DATA AVAILABILITY STATEMENT: The data that support the findings of this study are openly available in Hal Sorbonne Université at https://hal-sorbonne-universite-fr.ezproxy.u-pec.fr/.

References

Beresford, W. A. (1981). Chondroid bone, secondary cartilage, and metaplasia. Baltimore, Md: Urban & Schwarzenberg.

Brochu, C. A. (1999): Phylogenetics, Taxonomy, and Historical Biogeography of Alligatoroidea, Journal of Vertebrate Paleontology, 19, 9-100.

Bronzati M., Montefeltro, F. C., Langer, M. C. (2015). Diversification events and the effects of mass extinctions on Crocodyliformes evolutionary history. *Royal Society open science*, 2, 140385.

Buffrénil, V., Clarac, F. M., Fau, M., Martin, S., Martin, B., Pellé, E., & Laurin, M. (2015). Differentiation and growth of bone ornamentation in vertebrates: a comparative histological study among the Crocodylomorpha. *Journal of Morphology*, 276, 425–445.

Buffrénil, V., Dauphin, Y., Rage, J. C., & Sire, J. Y. (2011). An enamel-like tissue, osteodermine, on the osteoderms of a fossil anguid (Glyptosaurinae) lizard. *Comptes Rendus Palevol*, 10, 427–437.

Buffrénil, V., Sire, J-Y, & Rage, J-C. (2010). The histological structure of glyptosaurine osteoderms (Squamata: Anguidae), and the problem of osteoderm development in squamates. *Journal of Morphology*, 271, 729–37.

Burns, M. E., Vickaryous, M. K., Currie, P. J. (2013). Histological variability in fossil and recent alligatoroid osteoderms: systematic and functional implications. *Journal of Morphology*, 274, 676–686.

Castro, M. C., Montefeltro, F. C., Langer, M. C. (2014). The Quaternary vertebrate fauna of the limestone cave Gruta do Ioiô, northeastern Brazil. *Quaternary International*, 352, 164–175.

Cerda, I. A., & Desojo, J. B. (2011). Dermal armour histology of aetosaurs (Archosauria: Pseudosuchia), from the Upper Triassic of Argentina and Brazil. *Lethaia*, 44, 417– 428.

Cerda, I. A., Desojo, J. B., & Scheyer, T. M. (2018). Novel data on aetosaur (Archosauria, Pseudosuchia) osteoderm microanatomy and histology: palaeobiological implications. *Paleontology*, 61, 721–745.

Cerda, I. A., Sterli, J., & Scheyer, T. M. (2016). Bone shell microstructure of *Condorchelys antiqua* Sterli, 2008, a stem turtle from the Jurassic of Patagonia. *Comptes Rendus Palevol*, 15, 128–141.

Chen, I. H., Yang, W., & Meyers, M. A. (2014). *Alligator* osteoderms: mechanical behavior and hierarchical structure. *Materials Science and Engineering C*, 35, 441–448.

Chen, I. H., Yang, W., & Meyers, M. A. (2015). Leatherback sea turtle shell: A tough and flexible biological design. *Acta Biomaterialia*, 28, 2–12.

Chinsamy, A., & Raath, M. (1992). Preparation of fossil bone for histological examination. *Palaeontologia Africana*, 29: 39–44.

Clarac, F., Goussard, F., Teresi, L., Buffrénil, V., & Sansalone, V. (2017). Do the ornamented osteoderms influence the heat conduction through the skin? A finite element analysis in Crocodylomorpha. J*ournal of Thermal Biology*, 69, 39–53.

Dacke, C. G., Elsey, R. M., Trosclair, P. L., Sugiyama, T., Nevarez, J. G., & Schweitzer, M. H. (2015). *Alligator* osteoderms as a source of labile calcium for eggshell formation. *Journal of Zoology*, 297, 1–10.

Farlow, S., Hyashi, G., & Tattersall, G. J. (2010). Internal vascularity of the dermal plates of *Stegosaurus* (Ornithischia, Thyreophora), *Swiss Journal of Geosciences*, 103, 173–185.

Francillon-Vieillot, H., Buffrénil, V., Castanet, J., Géraudie, J.,Meunier, F. J., Sire, J. Y., Zylberberg, L., & Ricqlès, A. (1989). Microstructure and mineralization of vertebrate

skeletal tissues. In J. G. Carter (Ed.), *Skeletal biomineralization: Patterns, processes and evolutionary trends* (pp. 175–234). American Geophysical Union.

Fuchs, K., 2006. The Crocodile skin: The important characteristics in identifying. Edition Chimaira, Frankfurt, HE, Germany.

Girondot, M., & Laurin, M. (2003). Bone profiler: A tool to quantify, model, and statistically compare bone-section compactness profiles. *Journal of Vertebrate Paleontology*, 23, 458–461.

Godoy, P. L., M. Bronzati, E. Eltink, J. C. D. A. Marsola, G. M. Cidade, M. C. Langer, & F. C. Montefeltro. (2016). Postcranial anatomy of *Pissarrachampsa sera* (Crocodyliformes, Baurusuchidae) from the Late Cretaceous of Brazil: insights on lifestyle and phylogenetic significance. PeerJ 4, e2075.

Gônet, J., Laurin, M., & Girondot, M. (2022). "Bone Profiler: The next step to quantify, model and statistically compare bone section compactness profiles." *Paleontologica Electronica* In press.

Hill, R V. (2010). Osteoderms of *Simosuchus clarki* (Crocodyliformes: Notosuchia) from the Late Cretaceous of Madagascar. *Journal of Vertebrate Paleontology*, 30, 154–176.

Hill, R. V. (2005). Integrative morphological data sets for phylogenetic analysis of Amniota: The importance of integumentary characters and increased taxonomic sampling. *Systematic Biology*, 54, 530–547.

Inacio Veenstra, L. L. & Broeckhoven, C. (2022). Revisiting the thermo-regulation hypothesis of osteoderms: a study of the crocodilian *Paleosuchus palpebrosus* (Crocodilia: Alligatoridae). *Biological Journal of the Linnean Society*, 135, 679–691.

Klein, N. (2010). Long bone histology of Sauropterygia from the Lower Muschelkalk of the Germanic Basin provides unexpected implications for phylogeny. *PLoS ONE*, 5, e11613.

Kirby, A., Vickaryous, M. K, Boyde, A., Olivo, A., Moazen, M., Bertazzo, S., & Evans, S. (2020). A comparative histological study of the osteoderms in the lizards *Heloderma suspectum* (Squamata: Helodermatidae) and *Varanus komodoensis* (Squamata: Varanidae). *Journal of Anatomy*, 236, 1035–1043.

Laurin, M., Girondot, M., & Loth, M.–M. (2004). The evolution of long bone microanatomy and lifestyle in lissamphibians. *Paleobiology*, 30, 589–613.

Mannion, P. D., Upchurch, P., Carrano, M. T., Barrett, P. M. (2011). Testing the effect of rock record on diversity: a multidisciplinary approach to elucidating the generic richness of sauropodomorph dinosaurs through time. *Biological reviews of the Cambridge Philosophical Society*, 86, 157–181.

Marchetti, I., Delcourt, R., Tavares, S. A. S., Canalli, J. F., Nascimento, P. M., & Ricardi-Branco, F. (2022). Morphological and paleohistological description of a new Baurusuchidae specimen from the Adamantina Formation, Upper Cretaceous of Brazil. *Journal of South American Earth Sciences*, 114, 103693.

Marinho, T. S., Ribeiro, L. C. B., & Carvalho, I. S. (2006). Crocodylomorph osteoderms morphology from the paleontological site of Peirópolis (Bauru Basin, Upper Cretaceous). *Anuário do Instituto de Geociências*, 29, 44–53.

Molnar, J. L., Pierce, S. E., & Hutchinson, R. (2014). An experimental and morphometric test of the relationship between vertebral morphology and joint stiffness in Nile crocodiles (*Crocodylus nil- oticus*). *Journal of Experimental Biology*, 217, 758–768.

Montefeltro, F. C. (2019). The osteoderms of baurusuchid crocodyliforms (Mesoeucrocodylia, Notosuchia). *Journal of Vertebrate Paleontology*, 39, e1594242.

Moss, M. L. (1969). Comparative histology of dermal sclerifications in reptiles. *Acta Anatomica*, 73, 510–533.

Nyström, A., & Bruckner-Tuderman, L. (2019). Matrix molecules and skin biology. *Seminars in Cell and Developmental Biology*. 89, 136–146.

Ősi, A., Young, M. T., Galácz, A., & Rabi, M. (2018). A new large-bodied thalattosuchian crocodyliform from the Lower Jurassic (Toarcian) of Hungary, with further evidence of the mosaic acquisition of marine adaptations in Metriorhynchoidea. *PeerJ*, 6, e4668.

Ponce, D. A., Cerda, I. A., Desojo, J. B., & Nesbitt, S. J. (2017). The osteoderm microstructure in doswelliids and proterochampsids and its implications for palaeobiology of stem archosaurs. *Acta Palaeontologica Polonica*, 62, 819–831.

Ruiz, J. V., Bronzati, M., Ferreira, G. S., Martins, K. C., Queiroz, M. V., Langer, M. C., Montefeltro, F. C. (2021). A new species of *Caipirasuchus* (Notosuchia, Sphagesauridae) from the Late Cretaceous of Brazil and the evolutionary history of *Sphagesauria*. *Journal of Systematic Palaeontology*, Advance online publication.

Rutland, C. S., Cigler, P., Kubale Dvojmoč, V. (2019). Reptilian skin and its special histological structures. In: Rutland CS, Kubale Dvojmoč V, eds. Veterinary anatomy and physiology. Rijeka, Shanghai: InTech, 1–21.

Salisbury, S. W., & Frey, E. (2001). A biomechanical transformation model for the evolution of semi-spheroidal articulations between adjoining vertebral bodies in crocodilians. In: G. C. Grigg, Seebacher, F., & Franklin, C. E (Eds.), *Crocodilian Biology and Evolution* (pp. 121–148). Surrey Beatty & Sons.

Scheyer, T. M. (2007). Skeletal histology of the dermal armor of Placodontia: the occurrence of 'postcranial fibro-cartilaginous bone' and its developmental implications. *Journal of Anatomy*, 211, 737–753.

Scheyer, T. M., & Sánchez-Villagra, M. R. (2007). Carapace bone histology in the giant pleurodiran turtle *Stupendemys geographicus*: phylogeny and function. *Acta Palaeontologica Polonica*, 52, 137–154.

Scheyer, T. M., & Sander, P. M. (2004). Histology of ankylosaur osteoderms: implications for systematics and function. J*ournal of Vertebrate Paleontology*, 24, 874–893.

Scheyer, T. M., Danilov, I. G., Sukhanov, V. B., & Syromyatnikova, E. V. (2014). The shell bone histology of fossil and extant marine turtles revisited. *Biological Journal of the Linnean Society*, 112, 701–718.

Scheyer, T. M., Martin, Sander, P., Joyce, W. G., Böhme, W., Witzel, U. (2007). A plywood structure in the shell of fossil and living soft-shelled turtles (Trionychidae) and its evolutionary implications. *Organisms, Diversity and Evolution*, 7, 136–144.

Scheyer, T. M., Desojo, J. B., Cerda, I. A. (2014). Bone histology of phytosaur, aetosaur, and other archosauriform osteoderms (Eureptilia, Archosauromorpha). The Anatomical Record, 297, 240–260.

Seidel, M. R. (1979). The osteoderms of the American *Alligator* and their functional significance. *Herpetologica*, 35, 375–380.

Sena, M. V. A., Andrade, R. C. L. P., Sayão, J. M., & Oliveira, G. R. (2018). Bone microanatomy of *Pepesuchus deiseae* (Mesoeucrocodylia, Peirosauridae) reveals a mature individual from the Upper Cretaceous of Brazil. *Cretaceous Research*, 90: 335–348.

Sena, M. V. A., Bantim, R. A. M., Saraiva, A. A. F., Sayão, J. M., & Oliveira, G. R. (2020). Osteohistology and microanatomy of a new specimen of *Cearachelys placidoi* (Testudines: Pleurodira) a side-necked turtle from the lower Cretaceous of Brazil. *The Anatomical Record*, 304, 1294–1304.

Sena, M. V. A., Bantim, R. A. M., Saraiva, A. A. F., Sayão, J. M., Oliveira, G. R. (2021). Shell and long-bone histology, skeletochronology, and lifestyle of *Araripemys barretoi* (Testudines: Pleurodira), a side-necked turtle of the Lower Cretaceous from Brazil. *Anais da Academia Brasileira de Ciências*, 93, e20201606.

Skutschas, P. P., Boitsova, E. A., Cherepanov, G. O., & Danilov, I. G. (2017). Shell bone histology of the pan-carettochelyid turtle *Kizylkumemys schultzi* from the Upper

Cretaceous of Uzbekistan and shell bone morphology transformations in the evolution of pan-trionychian turtles. *Cretaceous Research*, 79, 171–181.

Vickaryous, M. K., & Hall, B.K. (2006). Osteoderm morphology and development in the nine-banded armadillo, *Dasypus novemcinctus* (Mammalia, Xenarthra, Cingulata). *Journal of Morphology,* 267, 1273–1283.

Vickaryous, M. K., & Hall, B. K. (2008). Development of the dermal skeleton in *Alligator mississippiensis* (Archosauria, Crocodylia) with comments on the homology of osteoderms. *Journal of Morphology*, 269, 398–422.

Vickaryous, M. K. & Sire, J. Y. (2009). The integumentary skeleton of tetrapods: origin, evolution, and development. *Journal of Anatomy*, 214, 441–464.

Vickaryous, M. K., Meldrum, G., & Russell, A. P. (2015). Armored geckos: a histological investigation of osteoderm development in *Tarentola* (Phyllodactylidae) and *Gekko* (Gekkonidae) with comments on their regeneration and inferred function. *Journal of Morphology*, 276, 1345–1357.

Vieira, L. G., Santos, A. L. Q., Moura, L. R., Orpinelli, S. R. T., Pereira, K. F., & Lima, F. C. (2016). Morphology, development and heterochrony of the carapace of giant amazon river turtle, *Podocnemis expansa* (Testudines, Podocnemidae). *Revista Pesquisa Veterinária Brasileira*, 36, 436–446.

von Baczko, M. B., Desojo, J. B., & Ponce, D. (2020). Postcranial anatomy and osteoderm histology of *Riojasuchus tenuisceps* and a phylogenetic update on Ornithosuchidae (Archosauria, Pseudosuchia) *Journal of Vertebrate Paleontology*, 39, e1693396.

Williams, C., Kirby, A., Marghoub, A., Kever, L., Ostashevskaya-Gohstand, S., Bertazzo, S., Moazen, M., Abzhanov, A., Herrel, A., Evans S. E., & Vickaryous, M. (2022). A review of the osteoderms of lizards (Reptilia: Squamata). *Biological Reviews*, 97, 1–19.

Witzmann, F., & Soler-Gijón, R. (2010). The bone histology of osteoderms in temnospondyl amphibians and in the chroniosuchian *Bystrowiella*. *Acta Zoologica*, 91, 96–114.

Woodward, H. N., Horner, J. R., & Farlow, J. O. (2014). Quantification of intraskeletal histovariability in *Alligator mississippiensis* and implications for vertebrate osteohistology. *PeerJ*, 2, e422.

Supplementary Material

Figure S1: Selected osteoderms of extinct crocodyliforms from Brazil before sectioning. A, Baurusuchidae indet. (LPRP/USP 0642); B, *Armadillosuchus arrudai* (LPRP/USP 0774); C, Bernissartiidae indet. (LAPEISA 026); D, *Caiman* sp. (LPRP/USP 0708); E, *Uberabasuchus terrificus* (CPPLIP 501); F, *Guarinisuchus* cf. *G. munizi* (CAV 0013-V); G, *Itasuchus jesuinoi* (CPPLIP 332); H, Baurusuchidae indet. (LPRP/USP 0634); and I, *Aplestosuchus sordidus* (LPRP/USP 0229-9). Scale bars: 1 cm.

Figure S2: Inner architecture of osteoderms viewed in cross section. Schematic black (bone) and white (vascular spaces and cavities) drawings of the extinct crocodyliforms prepared for use with the Bone ProfileR package. A, *Uberabasuchus terrificus* (CPPLIP 501); B, Baurusuchidae indet. (LPRP/USP 0642); C, *Itasuchus jesuinoi* (CPPLIP 332); D, Baurusuchidae indet. (LPRP/USP 0634); E, *Caiman* sp. (LPRP/USP 0708); F, *Armadillosuchus arrudai* (LPRP/USP 0774); G, *Aplestosuchus sordidus* (LPRP/USP 0229-9); H, *Mariliasuchus amarali* (MPM 087); I, *Guarinisuchus* cf. *G. munizi* (CAV 0013-V); and J, Bernissartiidae indet. (LAPEISA 026).

Table S1: Estimated bone compactness and relative bone wall thickness of studied bone elements of crocodyliform taxa.

Figure captions

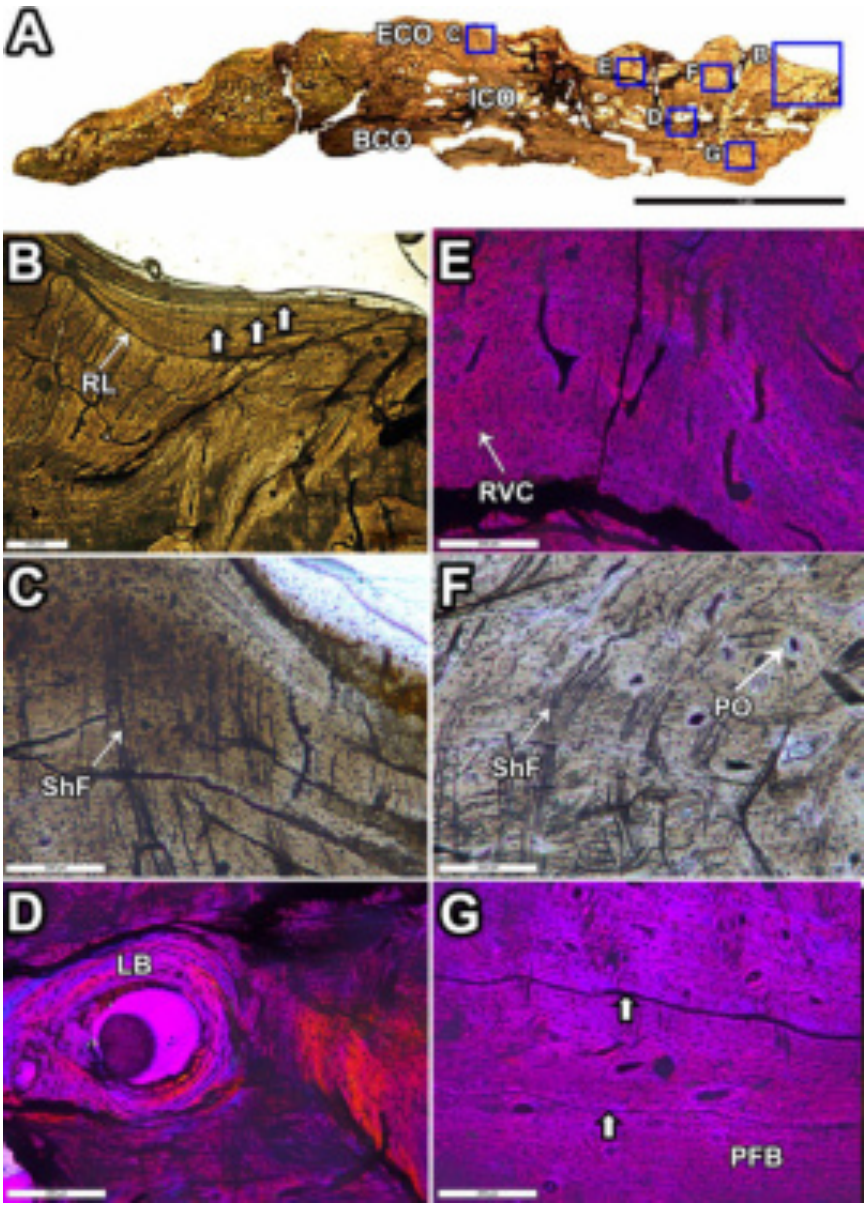

Figure 1: Histological section of an osteoderm of the notosuchian *Armadillosuchus arrudai* (LPRP/USP 0774) from Bauru Group, Brazil. A, Microanatomical overview of the thin section of the osteoderm. B, Note the presence of growth marks in the outermost cortex and a resorption line separating the two types of bone matrix. C, Long Sharpey's fibers oriented nearly perpendicularly to the outer surface. D, Close-up of the basal cortex exhibiting LAGs. E, Detail of remodeling process in the inner core of the osteoderm. F, Detail of the inner core showing short Sharpey's fibers. G, Close-up of the basal cortex interrupted by growth marks. Abbreviations: BCO, basal cortex; ECO, external cortex; ICO, inner core; LB, lamellar bone; PFB, parallel-fibered bone; PO, primary osteon; RL, resorption line; RVC, reticular vascular canal; ShF, Sharpey's fibers;

and White arrow, line of arrested growth. Images: Normal transmitted light (A, B, C and F) and polarized light with lambda compensator (E, D and G).

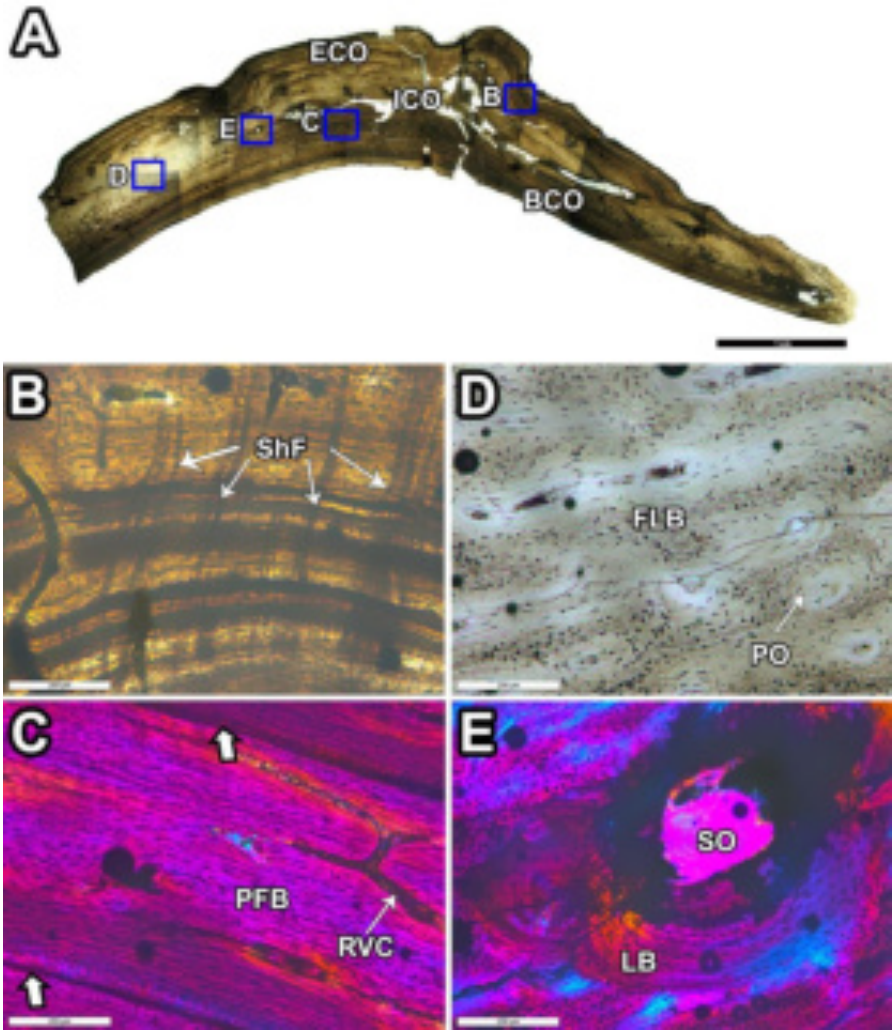

Figure 2: Histological section of an osteoderm of the notosuchian *Itasuchus jesuinoi* (CPPLIP 332) from Bauru Group, Brazil. A, Microanatomical overview of the perpendicular section of the osteoderm's ridge. B, Detail of Long Sharpey's fibers bundles oriented nearly perpendicularly to the outer surface. C, Parallel-fibered cortical bone interrupted by cyclical growth marks. D, Detail of the inner core formed by fibrolamellar bone. E, Isolated secondary osteon representing the remodeling process in the inner core. Abbreviations: BCO, basal cortex; ECO, external cortex; FLB, fibrolamellar bone; ICO, inner core; PFB, parallel-fibered bone; LB, lamellar bone; PO, primary osteon; RVC, reticular vascular canal; ShF, Sharpey fibers; SO, secondary

osteon; and White arrow, line of arrested growth. Images: Normal transmitted light (A–C) and polarized light with lambda compensator (C and E).

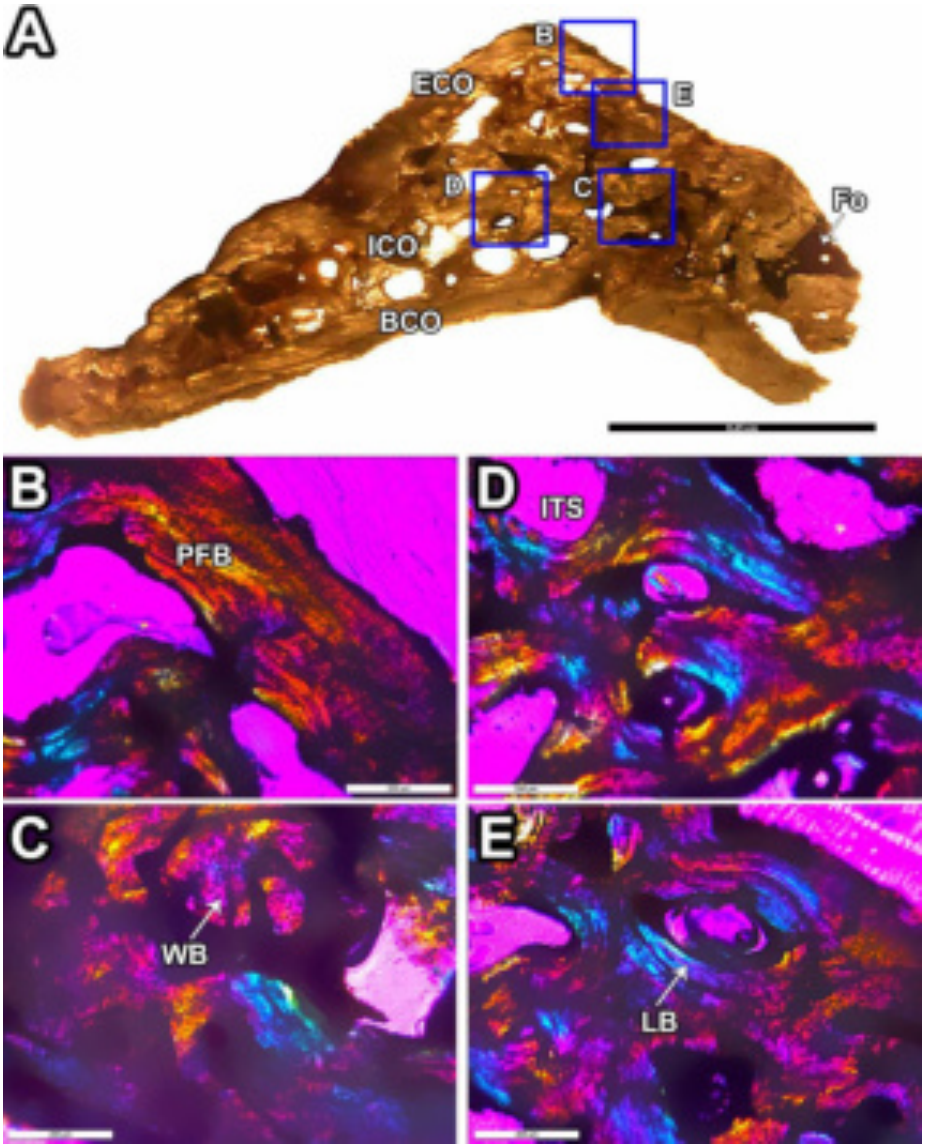

Figure 3: Histological section of an osteoderm of the notosuchian *Mariliasuchus amarali* (MPM 087) from Bauru Group, Brazil. A, Microanatomical overview of the perpendicular section of the osteoderm's keel. B, Detail of the external cortex constituted by disorganized parallel-fibered bone. C, Portions of woven bone in the inner core. and D, Secondary cancellous bone featured by short trabeculae. E, Lamellar bone surrounding the vascular spaces in the inner core. Abbreviations: BCO, basal cortex; ECO, external cortex; Fo, foramen; ICO, inner core; ITS, inter-trabecular space; LB,

lamellar bone; PFB, parallel-fibered bone; and WB, woven bone. Images: Normal transmitted light (A) and polarized light with lambda compensator (B–E).

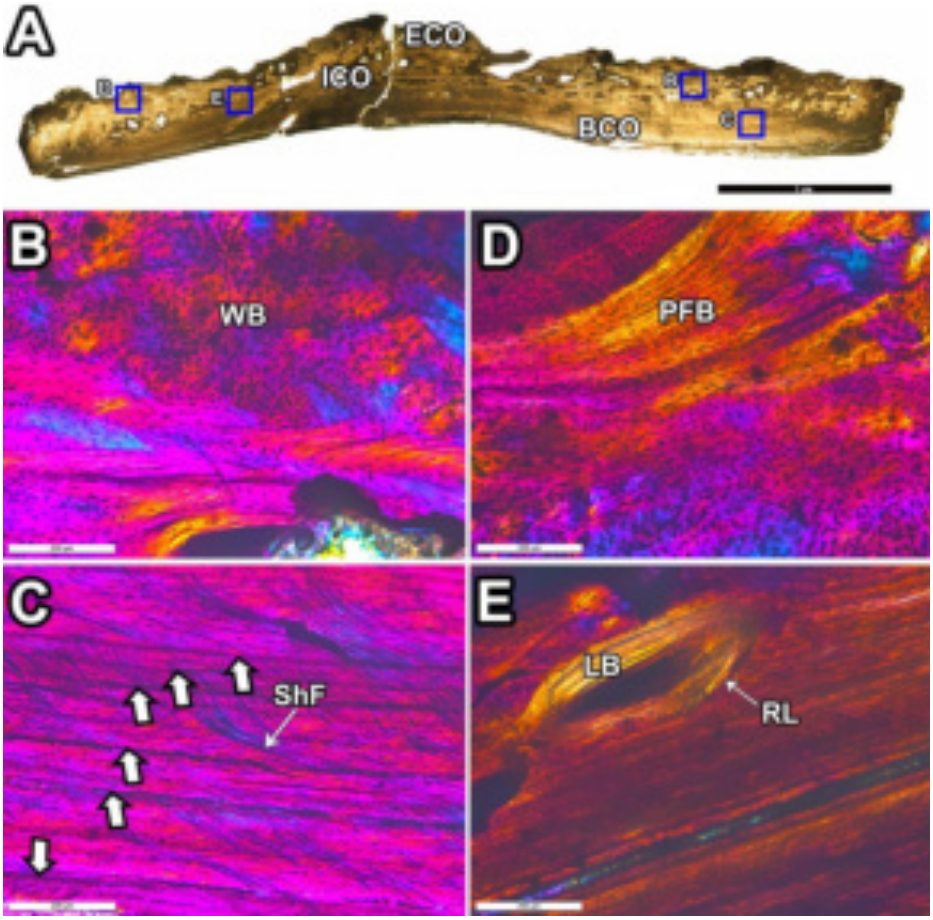

Figure 4: Histological section of an osteoderm of the notosuchian *Uberabasuchus terrificus* (CPPLIP 501) from Bauru Group, Brazil. A, Microanatomical overview of the thin section of the osteoderm. B, Close-up of the inner core composed of woven bone tissue with abundant osteocyte lacunae; C, Detail of the short Sharpey's fibers attached to growth lines. D, Close-up of the most external layer of the external cortex formed by parallel-fibered bone tissue. E, Close-up of the remodeling process expanding into the basal cortex. Abbreviations: AVC, anastomosed vascular canal; BCO, basal cortex; ECO, external cortex; ICO, inner core; LB, lamellar bone; PFB, parallel-fibered bone; PO, primary osteon; RL, resorption line; ShF, Sharpey's fibers; WB, woven bone and White arrow, line of arrested growth. Images: Normal transmitted light (A) and polarized light with lambda compensator (B–E).

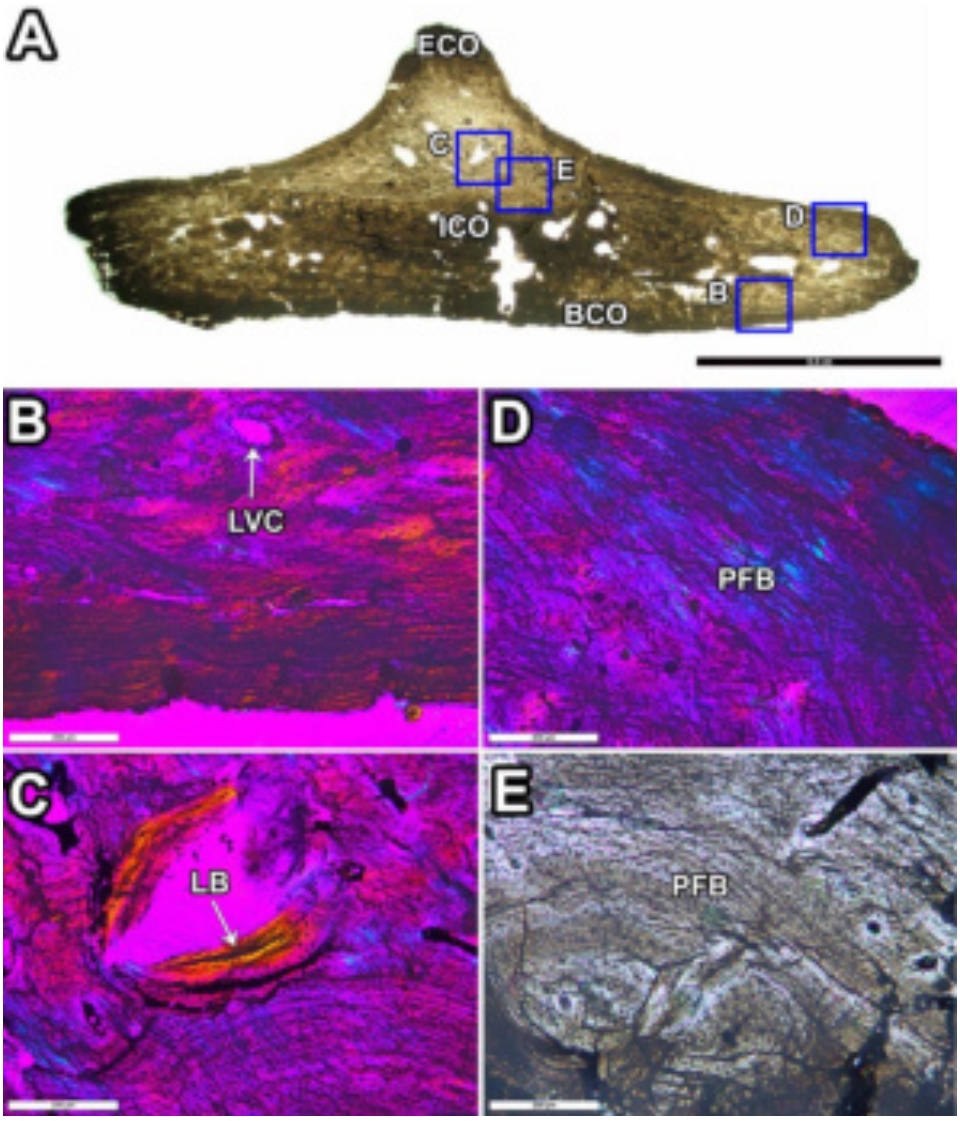

Figure 5: Histological section of an osteoderm of the notosuchian *Aplestosuchus sordidus* (LPRP/USP 0229-9) from Bauru Group, Brazil. A, Microanatomical overview of the perpendicular section of the osteoderm's keel. B, Slightly vascularized basal cortex showing mainly simple vascular canals. C, Note the remodeling process in the inner core. D and E, Close-up of the parallel-fibered bone tissue in external cortex and inner core. Abbreviations: BCO, basal cortex; ECO, external cortex; ICO, inner core; LB, lamellar bone; LVC, longitudinal vascular canal; and PFB, parallel-fibered bone. Images: Normal transmitted light (A and E) and polarized light with lambda compensator (B–D).

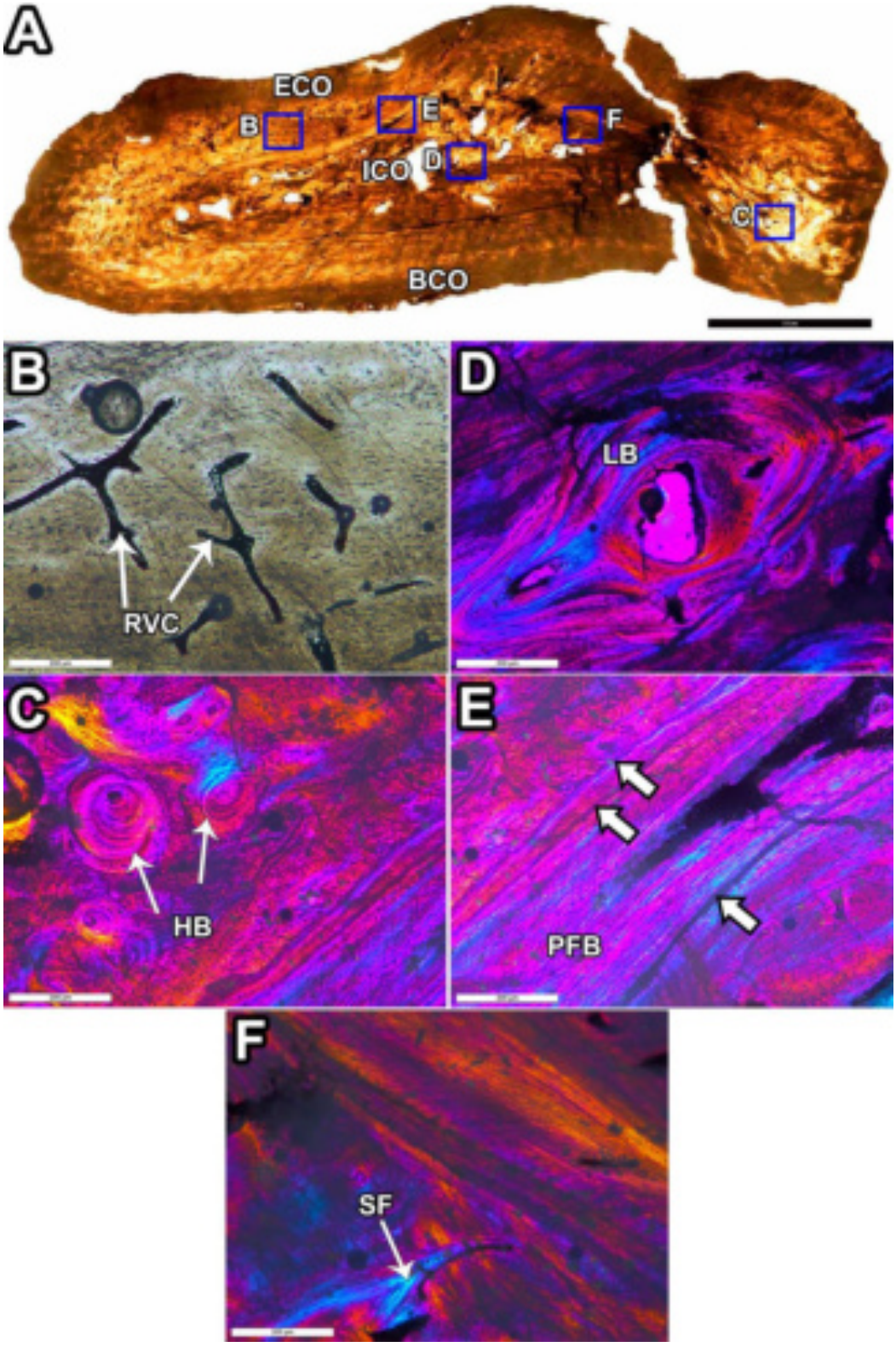

Figure 6: Histological section of an osteoderm of Baurusuchidae indet. (LPRP/USP 0634) from Bauru Group, Brazil. A, Microanatomical overview of the perpendicular section of the osteoderm's ridge. B, Reticular vascular pattern in the primary bone tissue. C, Detail of the inner core formed by Haversian bone. D, Secondary osteons anastomosed. E, Close up of primary bone with three cyclical growth marks preserved. F,

Detail of inner core showing structural fibers. Abbreviations: BCO, basal cortex; ECO, external cortex; HB, Haversian bone; ICO, inner core; LB, lamellar bone; PFB, parallel-fibered bone; RVC, reticular vascular canal; SF, structural fibers; and White arrow, line of arrested growth. Images: Normal transmitted light (A and B) and polarized light with lambda compensator (C–E).

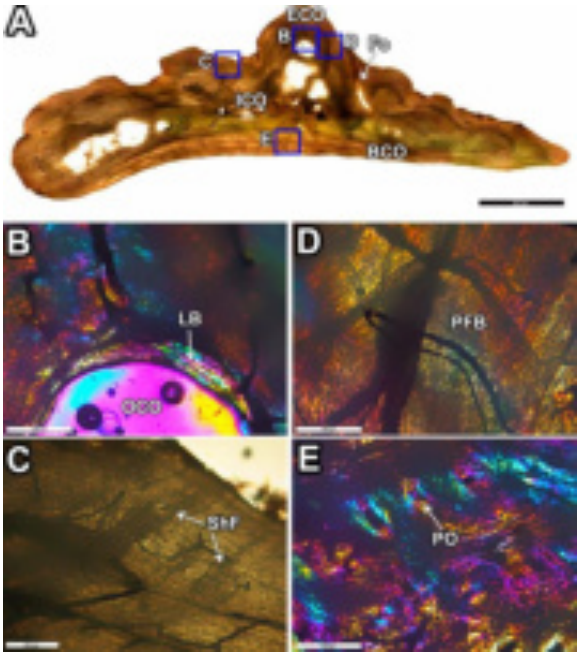

Figure 7: Histological section of an osteoderm of Baurusuchidae indet. (LPRP/USP 0642) from Bauru Group, Brazil. A, Microanatomical overview of the perpendicular section of the osteoderm's keel. B, Ossification center of the osteoderms surrounded by secondary lamellar bone tissue. C, Note the presence of numerous Sharpey's fibers perpendicularly oriented in the outermost part of the cortex. D and E, Detail of the disorganized parallel-fibered bone tissue. Abbreviations: BCO, basal cortex; ECO, external cortex; Fo, foramen; ICO, inner core; LB, lamellar bone; OCO, ossification center of osteoderms; PFB, parallel-fibered bone; PO, primary osteon and ShF, Sharpey's fibers. Images: Normal transmitted light (A and C) and polarized light with lambda compensator (B, D and E).

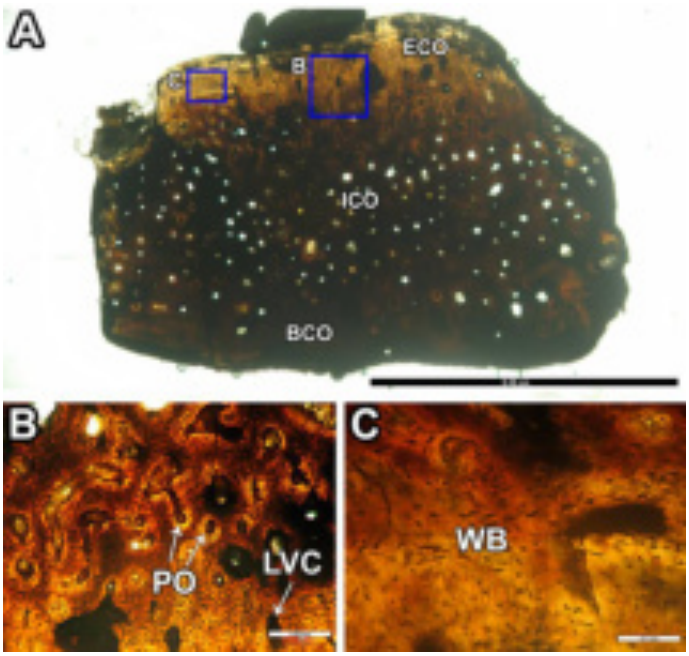

Figure 8: Histological section of an osteoderm of the neosuchian Bernissartiidae indet. (LAPEISA 026) from Alpercatas Basin, Brazil. A, Microanatomical overview of the fragmented osteoderms. B, Inner core is mainly vascularized by primary osteons and longitudinal vascular canals. C, Cortical bone seems to be formed by woven bone tissue. Abbreviations: BCO, basal cortex; ECO, external cortex; ICO, inner core; LVC, Longitudinal vascular canal; PO, primary osteon; and WB, woven bone. Images: Normal transmitted light.

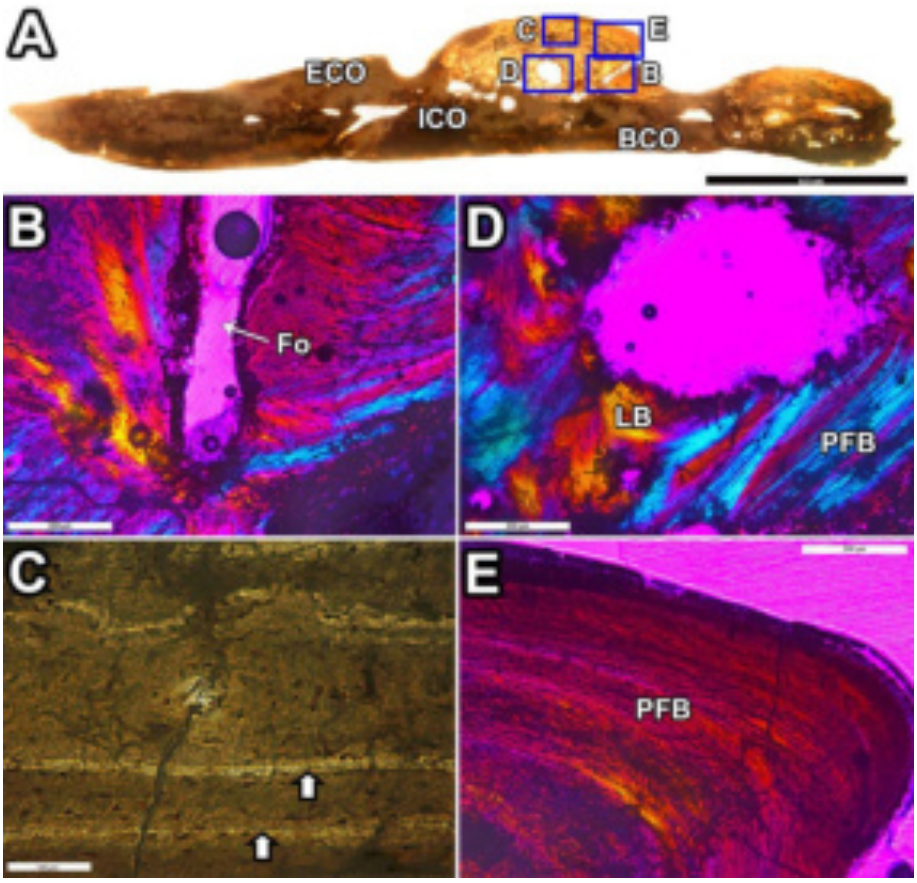

Figure 9: Histological section of an osteoderm of the neosuchian *Caiman* sp. (LPRP/USP 0708) from Gruta do Ioiô, Brazil. A, Microanatomical overview of the osteoderm's keel. B, Detail of a foramen situated in the bottom of the keel. C, Note two lines of arrested growth in the external cortex. D, Close-up of different orientations of the fibers bundles. E, Poorly vascularized parallel-fibered bone tissue. Abbreviations: BCO, basal cortex; ECO, external cortex; Fo, foramen; ICO, inner core; LB, lamellar bone; PFB, parallel-fibered bone; and White arrow, line of arrested growth. Images: Normal transmitted light (A and C) and polarized light with lambda compensator (B, D and E).

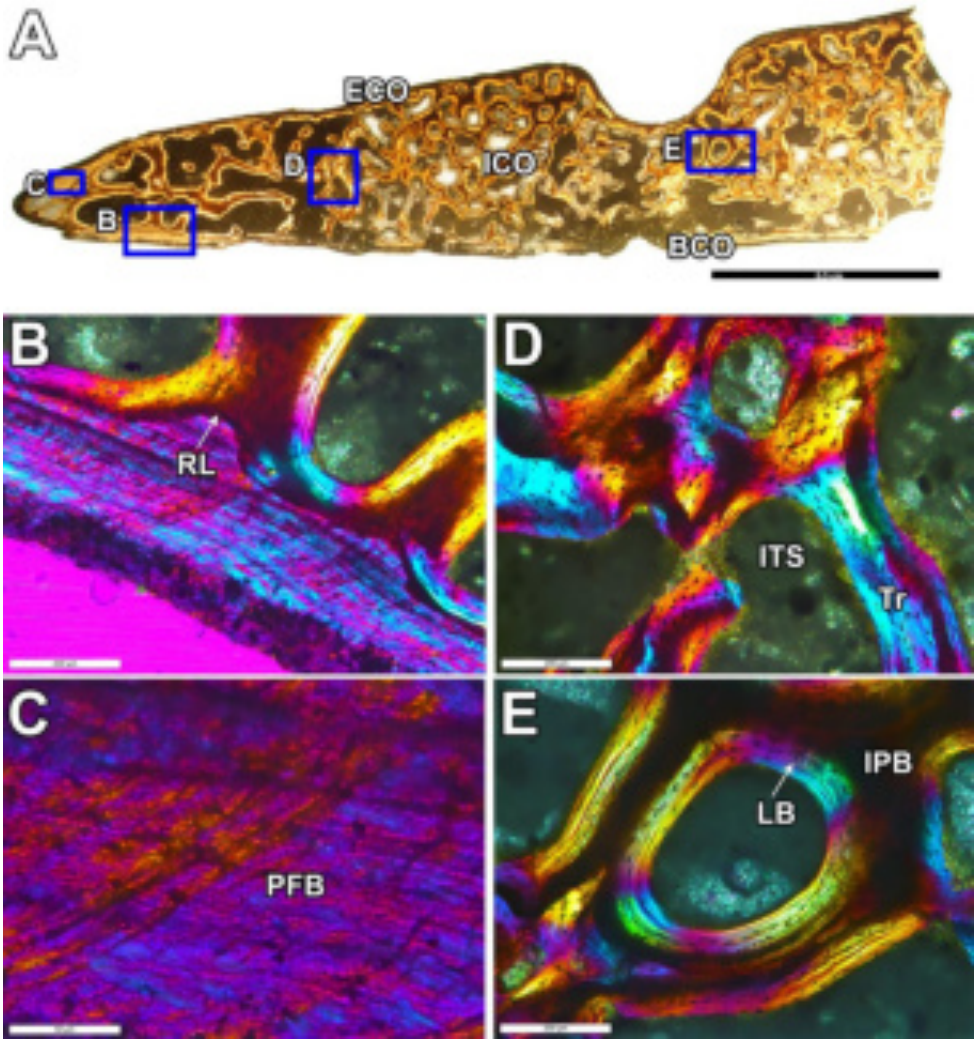

Figure 10: Histological section of an osteoderm of the neosuchian *Guarinisuchus* cf. *Guarinisuchus munizi* (CAV 0013-V) from Paraíba Basin. A, Microanatomical overview of the thin section of the osteoderm. B, Resorption line delimits the transition between basal cortex and inner core. C, Close-up of the thin cortex formed by parallel-fibered bone tissue. D, Trabecular bone tissue forms the intermediate layer. E, Interstitial primary bone is preserved inside the trabeculae. Abbreviations: BCO, basal cortex; ECO, external cortex; ICO, inner core; ITS, inter-trabecular space; IPB, interstitial primary bone; LB, lamellar bone; PFB, parallel-fibered bone; RL, resorption line; and Tr, trabecula. Images: Normal transmitted light (A) and polarized light with lambda compensator (B–E).